Turkish Journal of Physics

Volume 47 | Number 5 Article 3

2023

A portable and low-cost incubator system enabling real-time cell imaging based on a smartphone

ARİF ENGİN ÇETİN

TÜBİTAK

Turkish Journal of Physics

http://journals.tubitak.gov.tr/physics/

Research Article

Turk J Phys
(2023) 47: 279 – 296

doi:10.55730/1300-0101.2749

A portable and low-cost incubator system enabling real-time cell imaging based on a smartphone

Arif Engin ÇETİN*
Izmir Biomedicine and Genome Center (IBG), İzmir, Turkiye

Received: 10.08.2023 • **Accepted/Published Online:** 03.10.2023 • **Final Version:** 24.10.2023

Abstract: Incubators serve as essential tools for maintaining optimal temperature, humidity, and atmospheric gas composition for cell cultures. Their applications span across various fields like cell biology, microbiology, and molecular biology. However, in many cell-based studies, observing cellular changes often necessitates moving cells out of the incubator for microscope examination. Unfortunately, exposing cells to an environment that does not support healthy growth can undermine the reliability of test outcomes. In this article, we present a groundbreaking solution: a cost-effective, portable incubator system seamlessly integrated with a smartphone for real-time characterization tests. This innovation offers comparable imaging capabilities and maintains an environment similar to commercial microscope-incubator systems. Our system leverages a smartphone, enabling real-time cell tracking and data flow without the need for a complex and bulky computer-connected lens-camera arrangement. The inclusion of an incubator chamber within the smartphone ensures cells flourish in an optimal setting, while their growth remains unaffected by external factors. The compact design of the incubator system also ensures precise control and even distribution of the necessary cell culture media within the incubator. With these remarkable features, our system stands as a pioneering achievement—the first affordable and portable real-time cell tracking solution seamlessly integrated with a smartphone.

Keywords: Telemedicine, smartphone, incubator, cell imaging, confluency analysis

1. Introduction

The most essential device for cell-based studies is the incubator, which provides an environment where the cells to be used in these studies could carry out their proliferation in a healthy manner [1, 2]. However, the cellular environment provided by the incubators, e.g., 5% CO_2, 37 °C temperature, and 95% humidity, becomes unsuitable for proliferation when cells are taken out of the incubator and placed in a laboratory environment, causing a decrease in CO_2, heat, and humidity. In cell-based studies, the most important and time-consuming stage is the phase, where microscopic imaging systems are used to examine the findings of the applied methods [3]. During this lengthy process, subjecting cells to a different external environment affects the accuracy of experimental results due to the potential reactions of the cells to this change. This issue becomes even more critical when it comes to the prolonged real-time tracking of cells. In conventional cell culture studies, the cells under examination are maintained within an incubator environment. These cells are extracted from

*Correspondence: arifengin.cetin@ibg.edu.tr

the incubator environment and positioned onto an imaging platform during the imaging tests. In this stage, the following issues arise. Due to the noncoexistence of the incubator and the imaging platform within the same laboratory, the cell specimens utilized in tests could not be reintroduced into the incubator due to potential contamination issues. Consequently, challenges arise in follow-up tests reliant on imaging principles, often necessitating prolonged periods of observation. Another issue stems from the fact that cells removed from the incubator environment are exposed to a new milieu, inducing stress upon the cells. This stress could impact the tests conducted with agents meant to investigate effects on the cells, thereby compromising the integrity of the results obtained. Two commercial solutions have been introduced to address these two problems. (i) *Incubator-integrated microscopes:* microscopes with integrated cameras that are compact enough to fit within an incubator, enabling real-time imaging within the incubator environment. The drawback of this technology lies in the risk of contamination for the covered microscope system. In the setup, the enclosed microscope could not be removed from its sterile environment, as removing it and using it in external surroundings could increase the risk of contaminating the incubator housing live specimens. Furthermore, this technology is physically large and immobile, making it unable to be transported elsewhere if needed. (ii) *External incubators for microscopes:* compact incubators that could be integrated with camera-equipped microscopes, providing them with the capability for real-time imaging. The downside here is that the intensive conditions found in commercial incubator systems, such as 95% humidity and 5% CO_2 concentration, could be detrimental to electronic devices. To prevent damage, the microscope electronics must be waterproof, which turns out to be a costly technology. However, even with waterproofing, a microscope kept inside an incubator for extended periods might succumb to corrosion due to the humid and concentrated conditions, rendering it nonfunctional. Furthermore, attempting to fit microscopes into all existing incubators to facilitate imaging would not be feasible due to the varied interior volumes and designs of available incubators. Incubators on the market come in different sizes. For example, when attempting to place a microscope in a low-volume incubator like a drawered one, the removal of cells not currently being imaged and their placement in another incubator becomes necessary. In this scenario, additional incubator space would be needed for specimens not currently undergoing imaging.

In recent years, in addition to commercial solutions, various studies have been conducted to develop cost-effective systems for capturing real-time images while preserving the viability of cells [4, 5]. For instance, Walzik et al. (2015) developed a portable, long-term, and real-time microimaging platform [6]. In this system, cell imaging was accomplished using a motorized stage and a lens arrangement integrated with a camera. Images captured by the camera were tracked in real time using a computer, and the motorized stage was utilized to view different locations of the sample containing cells. While this system is portable, the components, e.g., custom-made microscope optics, camera system, computer, contribute to its high cost. Additionally, despite being lighter than commercial incubators and microscopes designed to work within them, the complexity and optical sensitivity of the setup compromise its portability [7]. A similar low-cost incubator system was developed by Rajan et al. [8]. In this study, a noncommercial and custom-made microscope setup was developed. A small incubator chamber was used to create a suitable environment for cell proliferation, enabling real-time imaging. However, the system's sophisticated optical-camera arrangement and dependence on a computer negatively affect both portability and cost. In both of these systems, the most significant issue is the limited ability to function in a nonlaboratory environment due to sophisticated engineering approaches. However, the cost of the optical focusing arrangement, camera, and computer-based imaging system used to capture and transmit images to end-users could be reduced by replacing this

system with a smartphone. Nowadays, smartphones, with their high magnification and resolution capabilities, have the potential to be used for microimaging. For example, Su et al. developed a portable biosensor system based on a smartphone that monitors cell viability for ochratoxin detection [9]. In another study, Yang et al. conducted cell migration analysis using a microfluidic system integrated with a smartphone [10]. These systems used the smartphone camera to visualize cell viability and track changes over time. With these capabilities, the need for sophisticated optical setups for sample imaging and computers for data processing is eliminated. However, currently, there is still no tracking system that uses a low-cost setup like a smartphone lens and a small-volume incubator for cellular imaging.

In this article, we developed an inexpensive and portable incubator system integrated with a smartphone, which could allow the culture, proliferation, and real-time characterization testing of cells without the need for a commercial incubator or a microscope-camera system placed within the incubator. Our system could provide similar imaging capabilities and incubation environment sustainability as commercial microscope-incubator systems. Our technology could significantly reduce production costs by using a smartphone to achieve real-time tracking of cells and data flow without the need for a sophisticated, heavy, and space-consuming computer-connected lens-camera system. Its small size and low weight could make it portable. The incubator chamber integrated with the smartphone ensures healthy cell proliferation, and desired changes could be tracked and reliable data produced without being affected by the external environment. The small size of the incubator system allows effective control of the environment required for cells and homogeneous distribution within the incubator. Moreover, the meaningful interpretation of images captured by incubator-integrated microscopes or microscopes supported by incubator chambers often requires the use of commercial software on a computer to obtain cellular information. Using our smartphone application and its image processing software, these pieces of information could be conveyed to the user on the same platform. Our system could be used in all locations with commercial incubators. Thus, samples taken out of the incubator may be placed within the system for image capture and then returned to the commercial incubator. The low cost of the system will pave the way for the proliferation of incubator-based imaging. Consequently, required tests for incubator parameters could be conducted in various setups, ensuring the reliability of these studies.

2. Materials and methods

2.1. Working principle of the technology

The developed system brings several significant advancements. Through the use of a smartphone, it enables real-time cell tracking and data flow, eliminating the need for a complex and space-consuming computer-connected lens-camera setup. This innovation drastically reduces production costs and offers a compact, lightweight design that enhances portability. The integration of an incubator chamber within the smartphone allows for healthy cell growth and the production of reliable data, shielded from external influences. The effectiveness of this approach is highlighted by the small volume of the incubator system, ensuring precise control over the cell environment and uniform distribution within the chamber. Furthermore, the technology also allows image processing on the same platform, enabling operations that are typically performed on a computer using separate software to be conducted through a cell analysis platform with incubator and imaging components, eliminating the need for any computer or commercial software. Figures 1a and 1b show the photograph and the 3-dimensional schematics of the imaging incubator system. Within the incubator platform responsible for real-time cell tracking

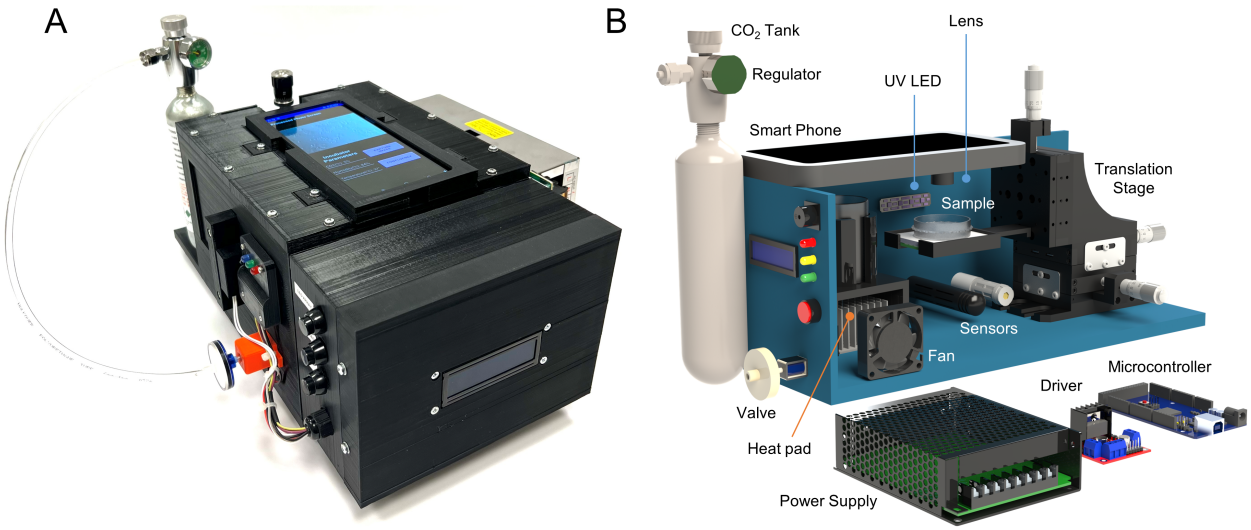

Figure 1. (A) Photograph and (B) schematic illustration of the portable and low-cost incubator system.

and data flow, samples (e.g., mammalian cells, bacteria) housed in a sample chamber are tracked using a smartphone. To capture reliable, high-resolution images, an optical focusing lens, specially designed for smartphones with low cost, is placed in front of the smartphone's lens. A micrometric stage capable of moving along the XYZ directions is used to visualize specific points on the samples and refine the image. This stage adjusts the distance between the sample chamber and the optical lens to enable imaging from different angles. An LED array light source beneath the sample chamber illuminates the samples. The regulation of this light source is facilitated by an electrical button integrated into the system's casing and connected to a microcontroller. Furthermore, our sample chamber has been designed with large space to accommodate diverse samples, including beakers and Petri dishes for observation. Additionally, the presence of the even illumination across the holder's surface with the use of the LED array ensures that, despite the large size of the sample holder, various regions within the sample holder can be uniformly illuminated.

The microcontroller controls the LED light source, heat pad, temperature-humidity, CO_2 sensors, and a safety valve (solenoid). This microcontroller is powered by a dedicated power supply. A built-in display on the microcontroller offers real-time information about temperature, humidity, and CO_2 levels inside the incubator to the user. To ensure a consistent maintenance of the optimal temperature, humidity, and CO_2 levels essential for cell growth within the incubator environment, a feedback mechanism has been established. Heat-humidity and CO_2 sensors controlled by the microcontroller are part of this mechanism. Furthermore, an integrated display provides real-time feedback to the user about the environmental conditions inside the incubator, including temperature, humidity, and CO_2 levels. This comprehensive setup ensures the provision of suitable conditions for cell culture within the incubator.

A heat pad beneath the sample chamber maintains the required temperature for cell growth (e.g., 37 °C) within the incubator chamber. To achieve a constant 37 °C temperature, the heat pad's emitted heat is monitored using a temperature and humidity (TH) sensor, managed by the microcontroller. Positioned near the sample chamber, the TH sensor continuously monitors the temperature. If the

ambient temperature exceeds 37 °C, the TH sensor detects this change and signals the microcontroller to deactivate the heat pad. Conversely, if the incubator's temperature drops below 37 °C, the microcontroller reactivates the heat pad to maintain the desired temperature. A water container placed above the heat pad evaporates deionized water to achieve the necessary humidity for cell growth. A temperature and humidity (TH) sensor, controlled by the microcontroller, regulates humidity levels within the incubator chamber. The TH sensor continually monitors humidity levels. When humidity falls below the desired threshold (indicating decreased water content within the chamber), an alert is issued to the user, prompting water container refilling to maintain appropriate humidity levels. A CO_2 tank supplies the required CO_2 for cell growth. A two-stage regulator maintains specific atmospheric pressure (e.g., 15 psi) within the incubator. A blend of 100% CO_2 from the tank and air evaporating from a water container achieves the needed CO_2 ratio for cells (typically around 5%). CO_2 levels are monitored using a CO_2 sensor controlled by the microcontroller. If CO_2 concentration surpasses 5%, a safety valve controlled by the microcontroller stops CO_2 flow. The safety valve includes a filter to prevent dust particle entry into the incubator. If CO_2 levels drop below the designated threshold, the microcontroller instructs the safety valve to reopen, restoring CO_2 flow into the incubator from the tank.

2.2. Design and installation of the electronic circuit

The system consists of electronic components and their associated circuits. In simple terms, the Arduino microcontroller is responsible for keeping track of the temperature and CO_2 levels using specific sensors. Based on the information gathered, it adjusts the conditions inside the incubator to ensure the cells remain at their best conditions. This involves managing the heating pad and a safety valve that could be connected to either the CO_2 source or the heating pad itself. The Arduino microcontroller has three main tasks: (i) it reads the data from the CO_2 sensor, (ii) reads data from sensors that measure temperature and humidity; and (iii) controls the driver for the 12V supply that is linked to both the heating pad and safety valve used in the system. The temperature and CO_2 sensors take readings three times and then calculate an average of these readings. Using average values helps smooth out any noise or variations that might arise from taking different readings in the same time interval, especially for the final reading. The measured values are then compared against a user-defined target or goal. If the measured temperature falls below the target temperature, the heaters are turned on. As the temperature approaches the set limit defined by the user, a gradual heating cycle begins. This cycle involves slowly turning the heating pad on and off in a predefined pattern. This process repeats until the desired temperature is achieved. If the measured CO_2 value falls below the desired level, the safety valve is activated. This valve then allows 100% CO_2 gas to flow from the CO_2 cylinder into the incubator. Once the CO_2 content matches the level set by the user, a specific cycle starts. During this cycle, the safety valve is opened and closed in a predefined pattern, and this open/close pattern continues until the desired CO_2 level is achieved.

CO_2 sensor: The CO_2 sensor used in the system operates based on nondispersive infrared (NDIR) technology, providing high selectivity and sensitivity to oxygen-depleted conditions. This sensor supports UART communication mode and is capable of measuring CO_2 levels in the range of 0 to 100,000 ppm. The SoftwareSerial.h library is employed for the CO_2 sensor protocol. This sensor is compatible with various microcontrollers equipped with UART ports, such as Arduino and Raspberry Pi. It finds widespread commercial use in applications including indoor air quality monitoring, industrial processes and safety monitoring, and agriculture and livestock production

process monitoring. The sensor is capable of reliable measurements after an initial heating period of three minutes.

Circuit connection: The sensor's outputs are connected to four pins on the Arduino microcontroller: GND (ground), 3.3-5.5VDC (supply voltage), Rx (data reception), and Tx (data transmission). The Tx and Rx pins of the sensor are respectively connected to digital pins on the Arduino.

Temperature-humidity sensor: The temperature-humidity sensor features a waterproof structure, and its accompanying PCB circuit is also waterproof, allowing it to operate without risk of malfunction even when submerged in water. The sensor incorporates an internal 10K pull-up resistor and a 0.1 µF filter capacitor. Consequently, it can be directly interfaced with an Arduino microcontroller. To measure and display temperature and humidity values, the Arduino utilizes the SHT20.h and Wire.h libraries. The sensor operates at a voltage range of 3.3V/5V and supports the I2C communication interface. The measurement range of the sensor is 0% to 100% RH (humidity) and –40 to 125 °C (temperature).

Circuit connection: The SCL (serial clock) pin on the Arduino is used to synchronize communication between the microcontroller and the sensor. The SDA (serial data) pin is employed for data exchange with the sensor.

LCD display module: This LCD display module utilizes the I2C communication protocol. Wiring an I2C LCD connection is much easier compared to connecting a standard LCD. Unlike a regular LCD display, this module, with its integrated circuit, can be connected to an Arduino board using just 4 pins (2 power, 2 communication) instead of the usual 12. The control and utilization of the LCD screen are facilitated through the use of the LiquidCrystal.h library.

LED light source (LED array): The LED array is composed of 1W white power LEDs. Within the 8×8 LED array, each power LED is connected to each other in parallel. The 8×8 power LED array is connected to Arduino's 3V pin and ground pin.

Driver board: The regulation of electric current and voltage within the system will be performed by a driver device named $L298N$. This driver will be powered by a 12V power supply, and the current value will range between 1.2 and 1.5 A. Digital pins connected to the driver will be responsible for controlling the Peltier device. Similarly, a digital pin connected to the driver will control the opening and closing of the air valve.

12V external power supply: Switch mode power supply (SMPS) is a type of power supply that operates with higher efficiency compared to traditional linear power sources and has a more compact structure. These types of power supplies are used to convert and regulate direct current (DC) voltage to desired levels and heights. They find extensive use, particularly in electronic devices and industrial applications. The 12V/2A and 5V/6A output SMPS used in the system take in alternating current (AC) input voltage on the primary side and transform this input voltage into a modulated signal at a high frequency through switching. This modulated signal is then stepped down or stepped up on the secondary side using a transformer, and converted to direct current voltage, resulting in regulated output voltages. While the 12V output can provide a maximum current of 2A, the 5V output can supply a maximum current of 6A. These current values are deemed sufficient and appropriate for this system.

Fan: The fan within the system will operate directly with a 12V supply voltage. This fan will be responsible for ensuring the homogeneous distribution of measured CO_2, temperature, and humidity values.

UV-C light: In the system, UV-C SMD LEDs with a wavelength range of 265–275 nm are used

for sterilization and disinfection purposes. This wavelength range belongs to the shorter wavelengths of the UVC region and has the ability to effectively damage the DNA and RNA of microorganisms. These LEDs are more compact, durable, and energy-efficient compared to traditional UV-C lamps. The SMD (Surface Mount Device) package type is known as an LED mounting style designed to facilitate assembly and integration processes. This feature further facilitates the integration of these LEDs into various applications.

2.3. PID control algorithm

For temperature control, the instantaneous temperature data sensed by the STH20 Temperature Humidity Sensor is transmitted to the analog pins of the Arduino Mega. This data is then utilized through a feedback circuit to drive the Peltier device connected to the L298N motor driver. The current through the Peltier device is adjusted based on its proximity to the target setpoint value, allowing for real-time temperature control. Humidity measurement is also performed using the same sensor, although humidity values are presented to the user solely through the LCD display without directly affecting the system. For CO_2 level control, a UART Infrared CO_2 Sensor is employed to detect CO_2 levels, and this data is acquired via the digital pins of the Arduino Mega. This information is utilized to determine the duration for which the Air Valve connected to the pressurized CO_2 cylinder will remain open. The Arduino Mega ensures balanced CO_2 distribution within the system in response to the CO_2 levels detected.

The parameters of the values to be checked are established alongside the variables defined within the code. To attain the target temperature of 37 °C, the most suitable $Setpoint\_T$ value is set at 38 °C. For PID control of both temperature and CO_2 control, separate K_p, K_i, and K_d values are determined. The deviation from the Setpoint value is denoted by the variables $error\_T$ for temperature and $error\_C$ for CO_2. The power delivered to the driver is characterized by the variables $power\_T$ for temperature control and $power\_C$ for CO_2 control. The Ki value accumulates minor errors over time to gradually steer the actuator towards the desired setpoint value. $errorSum$ variables are introduced to accumulate distinct errors. In case K_d values are applied, Kd_T and $difference\_T$ variables are defined for temperature, and Kd_C and $difference\_C$ for CO_2. The $difference$ variable signifies the variance between the prior value and the current value, leading to the establishment of $prev\_T$ for the former temperature value and $prev\_C$ for the former CO_2 value. These variables facilitate the computation of $difference$ values by deducting the current values from their preceding counterparts. The *voidsetup*() function initializes protocols and elucidates the function of the pins.

Instantaneous values are transferred to the $current_X$ variables through functions defined under the *voidloop* function. Within the loop, a counter is initialized, and *error* values derived from the target setpoint are subtracted and assigned to the corresponding variables. The *count* variable resets every 20 loops. Separate functions have been developed for temperature and CO_2 control.

Temperature control is accomplished by regulating the power delivered to the Peltier element. The specified power value for the Peltier, denoted as $power\_T$, is adjusted. Every 4 loops, if the *error* amount is 4 °C or closer to the setpoint, errors within $errorSum\_T$ are accumulated, and additionally, power proportional to $(errorSum_T)$x(Ki_T) is applied to the Peltier element. If the error value is 1 °C or less, the Ki_T value is reduced from 3 to 2 to prevent excessive oscillations and maintain a low $(errorSum)x(Ki\_T)$ value.

The $difference\_T$ value represents the difference between the previous and current values of the system. However, since the Kd_T value is zero, the power conveyed via $difference\_T$ has no

effect. The maximum power value that the Arduino Mega can sustain is 255 PWM. However, the Peltier element should be operated at a maximum of 5V. Therefore, even if the power value exceeds 190 PWM, it is constrained to approximately 5V, which corresponds to 190 PWM (referred to as $saturation\_T$), to ensure prolonged and reliable operation for the Peltier. If the power supplied to the Peltier element is below 190 PWM, this value is utilized to operate the Peltier.

When the target temperature is exceeded, the direction of the current delivered to the Peltier is reversed, and the heated surface starts to exhibit a cooling tendency. To maintain this balance, the value of $(saturation\_T)/2$ is added, as a sudden reversal of current direction is believed to potentially shorten the Peltier's lifespan.

CO_2 control is carried out according to the same principles as temperature control. One of the crucial points in CO_2 control is a situation arising from the system's continuous operation towards CO_2 depletion. Therefore, the CO_2 level is controlled only in the direction of increase. For CO_2 control, the transfer time of carbon dioxide from a pressurized cylinder at 1.5 atm pressure to the system is meticulously monitored. The CO_2 valve is designed to allow CO_2 flow for a maximum of 2 s.

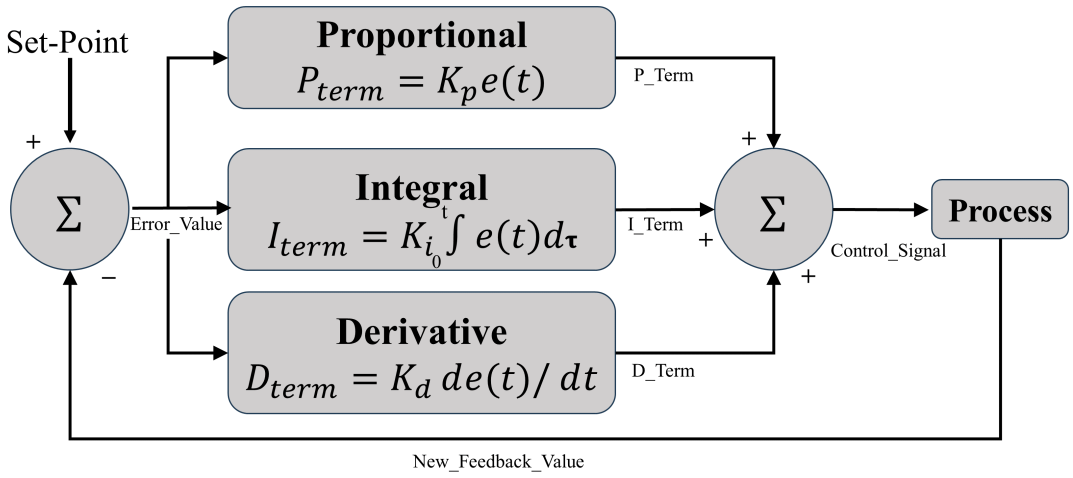

Figure 2. Schematic diagram of a proportional-integral-derivative (PID) control system.

2.4. Image processing algorithm

In addition to real-time cell monitoring, our technology can also be utilized to calculate an important parameter for cellular studies, which is cell confluency. Cell confluency refers to the degree to which a culture of adherent cells covers the surface of a growth vessel, typically a culture dish or flask. It indicates how much of the available surface area is occupied by cells. Cell confluency is usually expressed as a percentage. For example, if the surface of the growth vessel is completely covered by cells, the confluency would be 100%. If only half of the surface is covered, the confluency would be 50%, and so on. Cell confluency is an important factor in cell culture studies, as it can influence cell behavior, proliferation rates, and experimental outcomes. It is often used to determine the timing of cell passages (when cells need to be subcultured) and to ensure that cells are in the appropriate growth phase for specific experiments.

The algorithm for detecting confluency was developed using OpenCV. Initially, a preprocessing step was executed to eliminate background noise. The image is initially loaded in the BGR format and then converted to grayscale. This is essential for the impending binary thresholding processes. To avoid specific disturbances, particularly those of salt-and-pepper noise, an advanced technique termed 'Median Blur' is applied. In this technique, a nonlinear filter replaces each pixel's value with the median of its neighboring pixels. This technique is particularly effective against salt-and-pepper noise. Unlike Gaussian blur, it does not introduce any new pixel value, which is particularly beneficial when you want to preserve the edges in an image. After noise reduction, Adaptive Thresholding was applied. In this method, instead of a global value, the threshold value is the weighted sum of neighborhood values. The technique applied here is the Gaussian method, which determines the threshold of a pixel based on a weighted average of its surrounding pixels [11]. By using Gaussian function to create a filter that averages out the pixels in an image, the primary intention behind this blurring technique is to reduce image noise and detail. The neighboring pixels are given weights based on the Gaussian function, leading to a bell-shaped curve which gives higher weights to the closer pixels and lower weights to the faraway pixels. Mathematically, it can be represented as:

$$G(x,y) = \frac{1}{2\pi\sigma^2} e^{-\frac{x^2+y^2}{2\sigma^2}} \tag{2.1}$$

where σ is the standard deviation of the Gaussian distribution [12]. Morphological operations in image processing are fundamental techniques rooted in the principles of set theory, especially when applied to binary images, where images can be conceptualized as sets. Erosion aims to diminish the boundaries of the foreground object. When a kernel is positioned on a pixel in the original image, the resultant pixel will remain white only if every pixel underneath the kernel is white. Otherwise, it is set to black, effectively erasing minor white disturbances. In contrast, dilation seeks to expand the boundaries of the foreground object. If even one pixel under the kernel is white, the output pixel will be white, enhancing the size of the foreground feature. Opening is a two-step process of erosion followed by dilation, mainly utilized for noise elimination. Conversely, closing involves dilation followed by erosion, adept at sealing small voids or correcting darkened areas within an image object. These morphological operations underscore the application and relevance of set operations in refining and enhancing image quality [13].

The algorithm uses the Laplacian edge detection method that leverages the mathematical concept of the image's second derivative, known as the Laplacian, to pinpoint areas exhibiting rapid transitions, or edges [14]. Following this detection, contours are subsequently extracted from these identified edges. This method seeks to identify areas of rapid intensity change in an image, which are typically associated with edges. The Laplacian is a 2nd order derivative mask. In simple terms, if the first derivative (like Sobel or Prewitt) finds the slope (or rapid changes in intensity), the second derivative will find the zero crossings or the locations where the slope changes sign, marking an edge. The Laplacian can be expressed as:

$$\nabla^2 f = \frac{\partial^2 f}{\partial x^2} + \frac{\partial^2 f}{\partial y^2}. \tag{2.2}$$

Contours play a pivotal role in image processing, especially in the context of cellular microscopy [15]. They essentially trace the boundaries of distinct entities within an image, allowing for better delineation and interpretation of structures. In this process, the detected contours, which epitomize the

boundaries of cells, are meticulously rendered. Illustrating these contours serves a dual purpose: firstly, it provides a clear visual representation, facilitating easier identification and analysis of individual cells and their proximities. Secondly, by mapping these cellular boundaries, it aids in demarcating regions of confluency, wherein cells grow densely packed together. Understanding such regions is imperative for many biological and clinical applications as it provides insights into cellular growth patterns and behaviors. The detected contours (representing cell boundaries) are drawn. This helps in visual representation as well as in determining the regions of confluency. After identifying regions covered by cells, the confluency is calculated as the ratio of the area covered by cells to the total area. Mathematically, it is a ratio of the number of pixels inside the cell contours to the total number of pixels in the image.

$$Confluency(\%) = \frac{\text{Number of pixels that correspond to the cell area in the image}}{\text{Total number of pixels in the image}} * 100 \qquad (2.3)$$

By following this pipeline, the algorithm identifies cell clusters in microscopic images and computes the cell confluency, which can be crucial for biomedical studies and research.

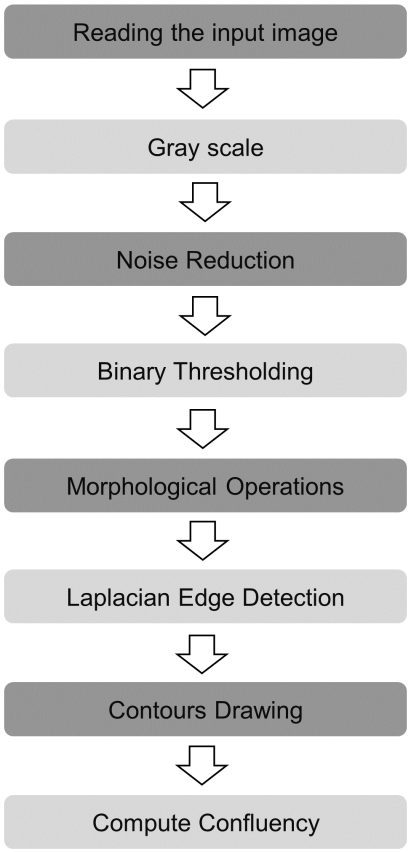

Figure 3. Flowchart of the image processing algorithm for cell confluency calculation.

3. Results

3.1. Maintaining incubator parameters

CO_2: When the CO_2 content of the incubator falls below 94% of the setpoint (e.g., 4.7% for a setpoint of 5%), the safety valve is opened to allow 100% CO_2 from the tank to be released into the incubator. Since the tank contains 100% CO_2 and the desired CO_2 level in the incubator's internal environment is 5%, the safety valve is only left open for 0.2 s (200 ms). The opening and closing cycle of the safety valve continues until the setpoint is reached. This approach allows the CO_2 content to rise to the setpoint while preventing it from exceeding the desired level. The average carbon dioxide concentration in the air is about 0.04%. In the figure, gas is introduced into the environment from the 6th minute to reach a CO_2 concentration of 5%. The CO_2 concentration is maintained steady for about 6 min and then the gas supply is cut off. As seen, the CO_2 concentration gradually decreases towards the amount of CO_2 naturally present in the air. Figure 4A demonstrates the response of a system utilizing a sensor-valve feedback mechanism. As shown, when the valve closes, the CO_2 concentration drops to the levels defined by the setpoint. The feedback mechanism then issues a directive for the valve to open, raising the CO_2 concentration back to the desired level, thereby maintaining the CO_2 concentration level. As shown in the figure, CO_2 level is kept around 5% with a 0.1% deviation range.

Temperature: Arduino control code has been programmed to measure the average temperature from the temperature-humidity sensor and activate the heaters if the average temperature falls below the setpoint. Heating is controlled in two ways. If the temperature is below 90% of the setpoint (e.g., with a setpoint of 36.9 °C, if the temperature drops to 33 °C), the heaters are continuously turned on. If the temperature is above 90% of the setpoint, the heaters are only turned on for 0.5 s and another reading is taken. This cycle continues until the setpoint is reached. This approach ensures that the system reaches the setpoint while preventing the incubator's internal environment from overheating beyond the desired level. As shown in Figure 4B, temperature level is kept around 37 °C with a 0.2 °C deviation range.

Humidity: By providing a consistent heat determined according to the incubator's internal volume through a heating pad, the aim is to maintain the internal environment of the incubator at a constant temperature while targeting a humidity level of $>80\%$. As seen in Figure 4C, the desired humidity level is achieved within a span of 8–10 min, after which the humidity remains stable at 82%. Similar to commercial incubators, when the humidity level falls below 81% (the humidity value is continuously displayed in real-time on the LCD screen), the user will refill the water container with deionized water to restore the humidity level.

In our technology, setting the relevant digital pin on the Arduino to HIGH allows a transistor to trigger the relay switch with 5V from the Arduino. Once the switch is triggered, it can provide 12V power. Setting the digital pin to LOW turns off the switch. This way, the relay selectively supplies power to both the heating pad and the safety valve. Two identical relay switches are used to provide 12V power to the heating pad and safety valve. A 2-channel 5V relay board has two independent relays and is compatible with development boards like Arduino. The optocouplers on the board allow isolation between the relay and the microcontroller board. This safeguarding protects the microcontroller board and computer USB interface against potential contact errors.

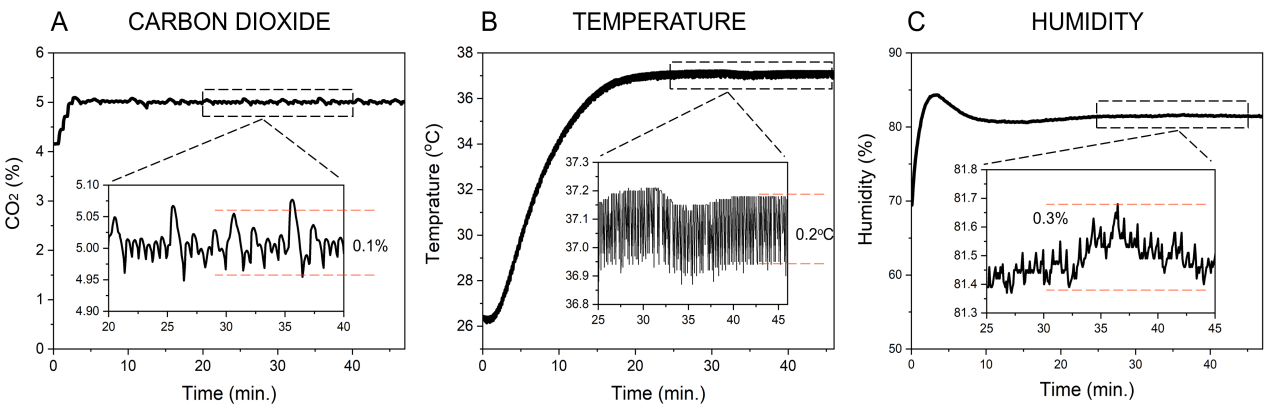

Figure 4. Capability of our incubator technology in maintaining CO_2 at 5%, temperature at 37 °C, and humidity parameters for cell seeding. (A) Sensor-valve feedback mechanism. (B) Sensor-heating pad feedback mechanism. (C) Ensuring the continuity of humidity level through the heating pad.

3.2. Confluency calculation results

To meticulously determine the optical resolution of the imaging module, we conducted a comprehensive analysis using a 1951 USAF resolution test chart. The resulting images, showcased in Figure 5A, were captured utilizing the camera at both 75X (Figure 5A-left figure) and 335X (Figure 5A-middle figure) magnifications. For an in-depth assessment, we scrutinized the intensity profiles of Group 7 (highlighted by the red box in Figure 5A-left) and Group 8, Element 1 (highlighted by the red box in Figure 5A-middle) of the USAF 1951 resolution test chart. This scrutiny allowed us to establish a precise optical resolution. The intensity profile of Group 7 is represented by the black curve in Figure 5A-right, while the intensity profile for Group 8, Element 1 (characterized by 1.95-µm-wide lines), is depicted by the red curve in the same figure. The evident differentiation between the horizontal and vertical lines within the eighth group and the first element points to an optical resolution of 256.0 line pairs per millimeter, which translates to an optical resolution of 1.95 µm.

Utilizing a microruler with interstripe distances of 0.1 mm, we precisely determined the actual magnification capabilities of our imaging setup, which encompasses the smartphone camera, the front lens, and the ingeniously positioned cheap lens externally used within the technology. The photograph of the microruler, taken by the smartphone with a digital zoom of 10x, is presented in Figure 5A-inset. Through a calibration study involving imaging the ruler at various magnifications, we derived a relationship between the actual magnification achieved by the imaging technology and the digital magnification exhibited by the smartphone. Specifically, this relationship is expressed as: Real = 7.4488 * Digital - 0.131. Given the maximum digital zoom capacity of the smartphone, which is 60x, we can thereby ascertain a magnification capacity of 450x.

To test our technology, we used human breast cancer cells (MCF-7). Figure 5B displays the confluency results of the MCF-7 cells seeded for 2 and 3 days, respectively. The initial cell concentration was set at 50,000 cells/mL. Our confluency algorithm successfully distinguished the difference between the two seeding durations, resulting in 54% versus 67%. The figure also demonstrates that our image processing algorithm could accurately determine the location of the cell clusters (highlighted in green in the figure).

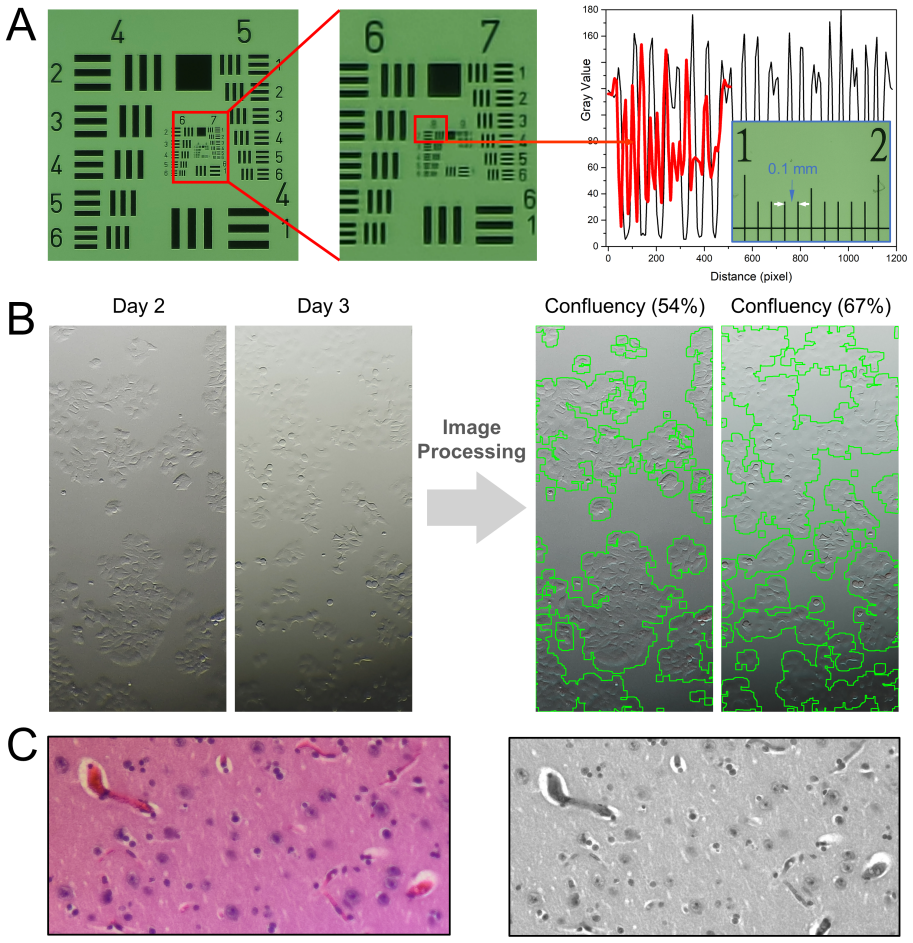

Figure 5. (A) Images of the USAF 1951 test chart captured at different magnifications. Intensity profiles of Group 7 (black curve) and Group 8, Element 1 (red curve). Inset in the figure shows a photograph of a microruler used to determine the technology's magnification capacity. (B) Images of MCF7 cells captured on day 2 and day 3. (C) Comparison between our imaging technology and a commercial microscope camera using tissue slide images.

Moreover, owing to its high-resolution capability, our imaging technology proves adept at visualizing a diverse array of biological samples. For instance, as illustrated in Figure 5C, we compare an image of a tissue slide acquired through our technology with one captured using a commercial microscope camera. This figure effectively highlights how our cost-effective imaging methodology, employing a smartphone camera and an economical lens, is proficient in delivering image quality akin to that achieved by a high-resolution microscope camera.

3.3. Smartphone application

The Android application is designed to improve the efficiency and simplicity of laboratory experiments. Developed using Java in Android Studio, this application offers advanced image processing capabilities and a real-time experience by exchanging data through USB with humidity, temperature, and CO_2 sensors connected to Arduino.

3.3.1. Key features

- **Cable connection and control:** The application can establish communication with external devices through cable connections. CO_2, humidity, and temperature data are transmitted to the application via USB connection with Arduino. The application processes this data and displays it visually in designated areas on the screen. These critical parameters are presented to users in the $IncubatorParameters$ section.

- **Advanced camera control:** Within the application, the $CameraActivity$ class enables image analysis using the device's camera. This feature, compatible with the Camera2 API library, allows for capturing, storing, and analyzing cell images. Functions like automatic focus and camera zoom enhance the user experience. Captured images can be easily saved using the $CaptureImage$ button.

- **Image analysis and scaling:** The application initiates the image processing algorithm through the $Confluency$ button. Integration with the OpenCV library enables the calculation of $confluency$. Data obtained from Arduino, through permissions defined in the AndroidManifest file, is processed within the application.

3.4. Utilized technologies and features

- **USB communication:** Data from humidity, temperature, and sensors connected to Arduino is received through USB serial communication. This ensures reliable data exchange.

- **Image processing:** The application manages camera functionality using Android's camera APIs. Additionally, Bitmap and Canvas elements are utilized for image analysis and processing.

- **Permission management:** User privacy and security are prioritized, with the application managing necessary permissions. The app requests required permissions from users when needed, as defined in the AndroidManifest file.

- **User interface design:** The application offers a user-friendly experience by effectively utilizing Android's user interface components, including buttons, text fields, and dialog boxes.

- **Camera control:** Android's Camera2 API is utilized to manage camera features. This API enables functions like automatic focus, camera zoom, and image quality adjustments within the application.

- **Image analysis:** The OpenCV library enables annotation, scaling, and analysis of images. This library is integrated into the application to execute the $confluency$ calculation.

The confluency application introduces an innovative approach to enhancing laboratory experiments. With its user-friendly interface, advanced image processing capabilities, and USB Arduino integration, it aims to streamline and improve laboratory experiences. Figure 6A displays the main screen of our smartphone application, featuring the incubator parameters and a real-time image of the cells adhered to the holder. Figure 6B demonstrates the outcome of our confluency algorithm executed on our smartphone application.

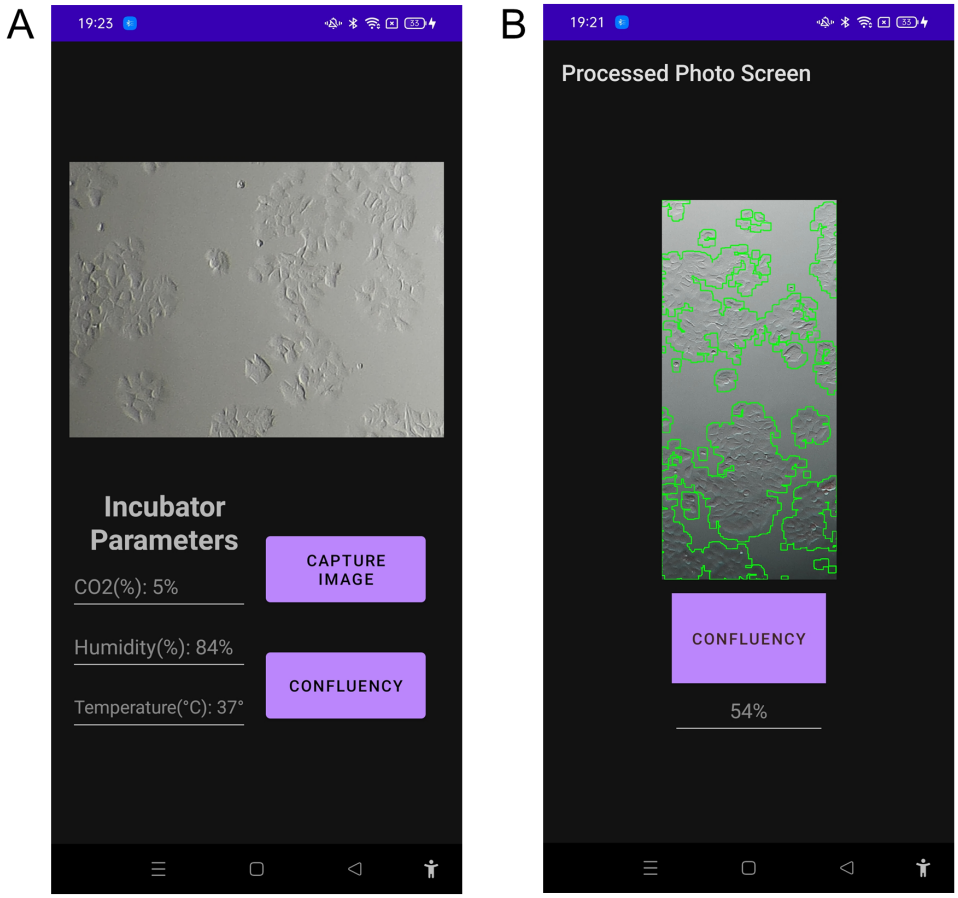

Figure 6. Primary screen of the smartphone application, displaying incubator parameters and portraying real-time images of cells adhered to the holder. (B) Results of the confluency algorithm on the smartphone application

4. Future directions

In this article, we present the inaugural prototype of our technology, which furnishes precise insights from cellular samples under meticulously controllable incubator parameters. As we progress towards commercialization, we intend to embark on additional advancements encompassing both hardware and software domains.

(i) To improve the precision of maintaining incubator conditions around the sample, we will decrease the volume of the incubator volume surrounding the sample compared to the initial design. To achieve this, we will develop a new incubating box that will be housed within the system casing. The system casing acts as a barrier, preventing the interaction between the external atmosphere and the controlled incubation environment. This new incubating box will serve as a secondary barrier, enhancing the isolation between the external environment and the incubation atmosphere by blocking any potential interactions. This strategic reduction in external interaction will significantly minimize fluctuations in incubator parameters, e.g., CO_2 level, temperature, and humidity. The incubating box will be attached to the sample holder, which is positioned on the translation stage. This setup ensures that the incubating box moves along with the sample, allowing to monitor various sample

positions. Importantly, this movement prevents any collision between the incubating box and the focusing lens in front of the smartphone lens. By designing a compact incubating box, we will achieve precise control over incubator parameters with minimal effort and energy consumption. This results in reduced reliance on heat pads and diminished CO_2 usage, contributing to overall energy efficiency. If necessary, the incubator box will be manufactured using insulating materials such as styrofoam to ensure enhanced isolation.

(ii) For the prototyping phase, we utilized a common material, polylactic acid (PLA), known for its ease of handling and cost-effective, quality manufacturing. However, as we transition toward commercialization, we will substitute this material with a biocompatible alternative that also offers superior mechanical support to the system's components. The electronic elements responsible for controlling incubator parameters, to be housed within the new incubating box, will be inherently biocompatible and could be easily disinfected using mild solvents like alcohol. The selection of biocompatible materials will align with these disassembly and decontamination specifications.

(iii) In the current design, the system casing occupies a considerable amount of space. However, with the introduction of a new incubating box, we will be able to confine the main hardware components to a smaller area. The remaining components will include the microcontroller and the electronic connections responsible for establishing communication between the controller and the incubating box. In this context, we will design a compact electronic card that will serve as a replacement for the intricate electrical connections that currently occupy significant space. Consequently, our updated system casing will exhibit a more compact form factor, resulting in an improved portable and lightweight platform.

(iv) Both the interior of the system casing and the incubating box will be made waterproof by employing biocompatible coating materials. We will also explore the possibility of utilizing materials that combine biocompatibility, waterproofing, and easy decompatibility, should the need arise.

(v) To improve visualization, we will incorporate image enhancement algorithms into our smartphone application, as we have previously introduced in the literature [16]. This integration will notably enhance the precision of our cell viability calculations. Additionally, we are conscientious about ensuring the compatibility of these algorithms with smartphone processors to facilitate efficient execution.

5. Conclusion

In conclusion, this article has successfully developed a novel real-time cell tracking system based on a smartphone-integrated incubator. The system demonstrated the capability to capture real-time images of samples within a Petri dish using a smartphone and a lens system placed in front of the smartphone camera. To ensure the ongoing viability of the imaged samples' vital functions, a microcontroller-based feedback mechanism was employed. This mechanism utilized a CO_2 sensor to regulate the flow of CO_2 from a connected tank into the incubator chamber, maintaining the CO_2 level based on sensor feedback. Similarly, an integrated heat pad controlled by a temperature-humidity sensor ensured precise temperature control within the incubator environment. The designed casing, manufactured using 3D printing technology, harmoniously integrated microcontroller-based electronic circuits and smartphone-based imaging components, facilitating seamless interaction between them. This pioneering system not only showcased the potential of real-time cell monitoring using a smartphone but also exemplified the successful integration of diverse technologies, resulting in a portable and functional solution for cell analysis. The article's outcomes open new horizons in the field of cellular studies, offering a practical and cost-effective approach to real-time monitoring and analysis of cell cultures.

Acknowledgment

A.E.C. acknowledges The Scientific and Technological Research Council of Türkiye (Project No. 119E308).

References

[1] Y. K. Jawale, U. Rapol and C. A. Athale, "3D-printed focussing mechanism for cellphone-based cellular microscopy," *Journal of Microscopy* **273** (2019) 105.

[2] V. Müller, J. M. Sousa, H. C. Koydemir, M. Veli, D. Tseng, L. Cerqueira, A. Ozcan, N. F. Azevedo and F. Westerlund, "Identification of pathogenic bacteria in complex samples using a smartphone based fluorescence microscope," *RSC Advances* **8** (2018) 36493.

[3] A. Orth, E. R. Wilson, J. G. Thompson and B. C. Gibson, "A dual-mode mobile phone microscope using the onboard camera flash and ambient light," *Scientific Reports* **8** (2018) 3298.

[4] N. A. Switz, M. V. D'Ambrosio and D. A. Fletcher, "Low-cost mobile phone microscopy with a reversed mobile phone camera lens," *Plos One* **9** (2014) e95330.

[5] H. Zhu, I. Sencan, J. Wong, S. Dimitrov, D. Tseng, K. Nagashima and A. Ozcan, "Cost-effective and rapid blood analysis on a cell-phone," *Lab on a Chip* **13** (2013) 1282.

[6] M. P. Walzik, V. Vollmar, T. Lachnit, H. Dietz, S. Haug, H. Bachmann, M. Fath, D. Aschenbrenner, S. A. Mofrad, O. Friedrich and D. F. Gilbert, "A portable low-cost long-term live cell imaging platform for biomedical research and education," *Biosensors and Bioelectronics* **64** (2015) 639.

[7] Q. Wei, H. Qi, W. Luo, D. Tseng, S. J. Ki, Z. Wan, Z. Göröcs, L. A. Bentolila, T. Wu, R. Sun and A. Ozcan, "Fluorescent imaging of single nanoparticles and viruses on a smart phone," *ACS Nano* **7** (2013) 9147.

[8] D. K. Rajan, J. Kreutzer, H. Välimäki, M. Pekkanen-Mattila, A. Ahola, A. Skogberg, K. Aalto-Setälä, H. Ihalainen, P. Kallio and J. Lekkala, "A portable live-cell imaging system with an invert-upright-convertible architecture and a mini-bioreactor for long-term simultaneous cell imaging, chemical sensing and electrophysiological recording," *IEEE Access* **6** (2018) 11063.

[9] K. Su, Y. Pan, Z. Wan, L. Zhong, J. Fang, Q. Zou and H. Li, "Smartphone-based portable biosensing system using cell viability biosensor for okadaic acid detection," *Sensors and Actuators B: Chemical* **251** (2017) 134.

[10] K. Yang, J. Wub, H. Peretz-Sorokab, L. Zhua, Z. Lia, Y. Sanga, J. Hipolitob, M. Zhangc, S. Santosd, C. Hillierc, R. L. de Fariac, Y. Liua and F. Linb, "Mkit: A cell migration assay based on microfluidic device and smartphone," *Biosensors and Bioelectronics* **99** (2018) 259.

[11] C. Li, F. Kulwa, J. Zhang, Z. Li, D. Tseng, H. Xu and X. Zhao, "A review of clustering methods in microorganism image analysis," *Information Technology in Biomedicine* **13** (2021) 13–25.

[12] I. T. Young and L. J.van Vliet, "Recursive implementation of the Gaussian filter," *Signal Processing* **44** (1995) 139.

[13] A. Raid, W. Khedr, M. El-dosuky and M. Aoud, "Image restoration based on morphological operations," *International Journal of Computer Science, Engineering and Information Technology* **4** (2014) 9.

[14] V. Berzins, "Accuracy of laplacian edge detectors," *Computer Vision, Graphics, and Image Processing* **27** (1984) 195.

[15] M. Ren, J. Yang and H. Sun, "Tracing boundary contours in a binary image," *Image and Vision Computing* **20** (2002) 125.

[16] Z. O. Yayci, U. Dura, Z. B. Kaya, A. E. Cetin and M. Turkan, "Microscale Image Enhancement Via PCA and Well-Exposedness Maps," *2022 IEEE International Conference on Image Processing (ICIP)* (2022) 2092.